Implications of Ocean Bottom Reflection for Internal Wave Spectra and Mixing

CHARLES C. ERIKSEN

Department of Earth, Atmospheric and Planetary Sciences, Massachusetts Institute of Technology, Cambridge, MA 02139

(Manuscript received 20 April 1984, in final form 22 March 1985)

ABSTRACT

A linear internal wave model for reflection off a sloping bottom applied to a field of horizontally isotropic waves typical of the deep ocean leads to a strongly perturbed frequency–vertical wavenumber energy spectrum. The spectrum is dominated by a nonintegrable singularity at the internal wave critical frequency characteristic of the environment and bottom slope. An observational requirement that the internal wave spectrum near the bottom relax to the open deep-ocean level and shape within a few hundred meters vertically implies a flux imbalance normal to the boundary. The flux that must be redistributed over the internal wave spectrum, or lost from it, amounts to $O(10^{-2}$ W $m^{-2})$, larger than for most other energy transfer mechanisms estimated for internal waves. A small fraction of this flux imbalance applied to mixing can account for a basin-averaged effective vertical diffusivity of 10^{-4} m^2 s^{-1}. Bottom reflection represents not only a likely and powerful sink for internal wave energy, but a mechanism that may be important to the oceanic general circulation through its contribution to mixing.

1. Introduction

Internal wave reflection from sloping bottom topography has been documented observationally at several sites where near-bottom measurements have been made (Eriksen, 1982). In all cases, the spectrum of internal wave motions is perturbed from its open deep-ocean form. (See the reviews by Munk, 1981; Olbers, 1983, for discussions of the spectrum of internal waves in the deep ocean away from boundaries.) The bottom-reflection perturbed spectrum exhibits strong enhancement and horizontal anisotropy over a band of frequencies centered at the frequency where rays are inclined the same as the bottom slope, i.e., the critical frequency. These features are predicted by linear theory. Within a few hundred meters of the bottom, the spectrum is observed to relax to the shape and level characteristic of the deep ocean interior. This adjustment is not predicted by linear theory. Rather, the adjustment must be due to nonlinear processes that redistribute internal wave energy throughout the spectrum and/or transform it into potential energy via mixing. The degree to which the internal wave spectrum is perturbed by bottom reflection and its implications are the subject of this theoretical study.

Near-bottom moored observations indicate spectral enhancement and cross-isobath alignment of motions near the critical frequency, but not to the degree predicted by linear theory. Spectral intensification decays roughly exponentially from the ocean bottom with a scale of about 100 m (Eriksen, 1982). Moored vertical-difference estimates of shear and buoyancy frequency near the bottom show that Richardson numbers over scales as large as 50 m have distributions which cut off at roughly Ri = 0.25 near the bottom from gradients enhanced by reflection. Profile measurements of currents also indicate near-bottom spectral changes. Hogg *et al.* (1978) found that the spectrum of vertical shear of horizontal currents is slightly diminished at vertical wavelengths longer than about a kilometer and somewhat enhanced at shorter wavelengths in approaching Bermuda from the open ocean at thermocline and subthermocline depths. Similarly, Johnson and Sanford (1980) found a transition from clockwise to anticlockwise polarization of horizontal current variance in the same data in approaching Bermuda, a transition that can be interpreted as one from a preponderance of downward to upward internal wave energy flux. They also found currents polarized normal to isobaths in shallower water. Although frequency spectra and vertical wavenumber spectra both show evidence for perturbations of the internal wave spectrum by reflection, the behavior of the joint frequency–wavenumber spectrum of internal wave motions near a sloping bottom has not been measured. Further substantial progress on the reflection process as it actually occurs in the ocean requires attempts to make such measurements.

The purpose of this study is to extend the results of single wave reflection from an arbitrary sloping plane bottom to reflection of a full spectrum of waves and examine the implications of such a calculation for processes of wave interaction both with other waves and with the mean stratification. We imagine flux of internal wave energy with a given spectrum

which is incident on a sloping bottom. The energy density of the total (incident plus reflected) wave field can be calculated from the reflection rules for single wave components. The basic problem for estimating the amount of internal wave energy involved in reflection is that linear theory leads to a nonintegrably singular energy spectrum for the wave field. However, since the observed total spectrum some distance off the bottom is not demonstrably different from the interior spectrum, a flux imbalance is implied between the incident and reflected parts of the wave field. The nature and strength of this flux imbalance is the ultimate subject of this study.

Some remarks on sea floor topography are in order since the distribution of bottom slopes in a range of horizontal scales has direct bearing on the importance of bottom reflection to the oceanic internal wave spectrum. Basically, for the scales of importance to internal waves, most of the ocean bottom is sloping rather than flat. Abyssal hills cover a sizeable majority of the ocean floor. According to Bell (1975a) the rms slope of the sea floor for horizontal wavenumbers less than 0.75 cpkm (cycles per kilometer) is 0.07. Slopes in the range 0.1–0.5 are common on islands and seamounts. Slopes at the low end of this range are typical for midocean ridges, which cover a sizeable portion of the sea floor. For a more detailed discussion of sea floor bathymetry, the reader is referred to Bell (1975b).

This paper is organized by reviewing the essential features of reflection of a single linear internal wave from simple sloping topography (Section 2), extending the results to a spectrum of waves (Section 3), and calculating the flux imbalances implied by the observations (Section 4). For a canonical spectrum of deep ocean internal waves, the latest version of the Garrett-Munk models for the internal wave spectrum is employed (Munk, 1981). In the final section, some critical underpinnings of the reflection problem are examined and the implications for deep-ocean internal wave processes are discussed. It appears that reflection may be a potent mechanism for mixing near ocean boundaries, which in turn may determine the effective vertical diffusivity of the ocean on basin scales.

2. Internal wave reflection model

The theory for reflection of linear internal gravity waves off a sloping plane bottom in a uniformly stratified, inviscid, Boussinesq, incompressible fluid has been presented by Eriksen (1982). His notation for developing a spectral model for reflection will be employed in this paper. Several salient characteristics of the reflection process relevant to the spectral calculation will be highlighted in this section.

The boundary condition at the sloping bottom is one of no normal flow. This precludes any pressure work normal to the boundary, thereby guaranteeing that waves conserve energy flux normal to the boundary in reflecting. Since the inclination of internal wave characteristics is independent of spatial scale, in order to satisfy this condition the waves must, in general, change wavenumber magnitude. They do this while preserving their wavenumber parallel to isobaths, leading to the following expressions for the ratio of reflected to incident vertical wavenumber m and azimuth ϕ

$$\frac{m_r}{m_i} = -\frac{\cos(\alpha - \theta_i)}{\cos(\alpha + \theta_i)} - \frac{\sin 2\theta_i \sin 2\alpha(\cos\phi_i - 1)}{2\cos(\alpha + \theta_i)\cos(\alpha - \theta_i)} \quad (1)$$

$$\phi_r = \sin^{-1}(|m_i/m_r| \sin\phi_i), \quad (2)$$

where $s = \tan\alpha$ is the bottom slope, $\tan\theta = m(k^2 + l^2)^{-1/2}$, (k, l, m) are the wavenumber vector components and subscripts i and r refer to incident and reflected values. Azimuth $\phi = 0$ corresponds to the onslope direction and $\tan\phi = k/l$.

When the incident internal wave characteristics are inclined the same as the bottom slope, reflected waves are unable to propagate away from the bottom. This singular case arises at the internal wave critical frequency σ_c defined by $\sigma_c^2 = (N^2 \sin^2\alpha + f^2 \cos^2\alpha) = (N^2 s^2 + f^2)/(1 + s^2)$ where f and N are the inertial and buoyancy frequencies, respectively. The two-dimensional problem of waves incident normal to isobaths towards shallower water ($\phi_i = 0$) has distinctly different character for $\sigma > \sigma_c$ and $\sigma < \sigma_c$. For $\sigma > \sigma_c$ the slope is transmissive ($\phi_r = 0$) but for $\sigma < \sigma_c$ the slope is reflective ($\phi_r = \pi$). For waves with nonzero alongslope wavenumber ($\phi_i \neq 0$), the possibilities are more complicated. They can be summarized with reference to the product of bottom slope and wavenumber slope $a = \tan\alpha\tan\theta_i$ by

Subcritical case: $\sigma < \sigma_c (|a| > 1)$

$$|\phi_i| \leq \cos^{-1}(-1/a) \quad \text{and} \quad |\phi_r| \geq \pi/2$$

$$\text{for} \quad \left\{ \begin{matrix} m_i > 0,\ a > 1;\ m_r/m_i \geq 1 \\ m_i < 0,\ a < -1,\ 0 \leq m_r/m_i \leq 1 \end{matrix} \right\}; \quad (3a)$$

Supercritical case: $\sigma > \sigma_c (0 < a < 1)$

$$\text{for} \quad |\phi_i| \left\{ \begin{matrix} \leq \\ \geq \end{matrix} \right\} \cos^{-1}[-2a/(a^2 + 1)] : |\phi_r| \left\{ \begin{matrix} \leq \\ \geq \end{matrix} \right\} \pi/2$$

$$\text{for} \quad |\phi_i| \left\{ \begin{matrix} \leq \\ \geq \end{matrix} \right\} \cos^{-1}(-a) : -m_r/m_i \left\{ \begin{matrix} \geq \\ \leq \end{matrix} \right\} 1; \quad (3b)$$

where $\pi/2 \leq \cos^{-1}(-a) \leq \cos^{-1}[-2a/(a^2 + 1)]$. The first of these relations (3a) states that for subcritical frequencies ($\sigma < \sigma_c$), reflected waves are directed toward deeper water regardless of incident azimuth and are shorter or longer than incident waves depending on whether the incident wave has downward or upward vertical wavenumber, respectively. At supercritical frequencies ($\sigma > \sigma_c$), relations (3b) state that reflected waves may be either shorter or longer

than incident waves and may be directed toward shallower water even if the incident wave travels toward deeper water (a phenomenon analogous to total internal reflection in other problems in physics). Special cases of "unamplified" waves (e.g., $m_r = \pm m_i$) may be found for both subcritical and supercritical frequencies. For supercritical frequencies when $\cos\phi_i = -a$, then $\phi_r = -\phi_i$ (as if the sloping boundary were a vertical wall). For subcritical frequencies when $\cos\phi_i = -1/a$, then $\phi_r = \phi_i$ (the incident wave just grazes the sloping bottom, not really reflecting, but just traveling parallel to a line in the plane of the sloping bottom). The properties of reflection that have profound effects on the form of the energy spectrum of a field of waves are that wavenumbers amplify differently depending on both frequency and incident azimuth and that some incident wave azimuths are precluded because they correspond to incident waves that would have to come up through the bottom slope for $\sigma < \sigma_c$ [i.e., $|\phi_i| > \cos^{-1}(-1/a)$].

The energy density of a reflected wave component E_r is related to the incident energy density E_i by

$$E_r/E_i = (m_r/m_i)^2. \tag{4}$$

This result can be derived from applying the no normal-flow boundary condition or, equivalently, by requiring incident and reflected energy flux to be equal and oppositely directed normal to the bottom. (In Section 4, this requirement will be relaxed in favor of assuming a fixed relation between E_r and E_i and inferring the flux imbalances which result.) The group velocity of internal waves is given by

$$\mathbf{c}_g = \cos\theta \sin^2\theta \frac{N^2 - f^2}{m\sigma} \times (\sin\theta \cos\phi \mathbf{x} + \sin\theta \sin\phi \mathbf{y} - \cos\theta \mathbf{z}) \tag{5}$$

where $\mathbf{x}$, $\mathbf{y}$, $\mathbf{z}$ are the unit vectors parallel to k, l, and m. Since the unit normal to the bottom is $\mathbf{n} = -\sin\alpha\mathbf{x} + \cos\alpha\mathbf{z}$, the flux normal to the bottom is

$$F_n = -E \cos\theta \sin^2\theta \frac{N^2 - f^2}{m\sigma} \times (\sin\theta\cos\phi\sin\alpha + \cos\theta\cos\alpha) \tag{6}$$

where F_n is defined as positive out of the bottom. It is the fact that flux (or group speed) varies inversely as wavenumber that leads to the energy density ratio (4) varying as the square of the wavenumber amplification. Simply stated, in order for a reflected wave to carry as much energy away from the boundary as was incident, its energy density must compensate for amplifications in both its group speed and ray tube width, each of which is inversely proportional to its vertical wavenumber amplification.

3. A spectrum of reflecting internal waves

From the kinematic effects of reflection of a single internal wave incident on a sloping bottom, the resulting spectral energy density for a given incident field of waves is not readily apparent. Aside from gross qualitative features (i.e., a peak in the frequency spectrum centered at the critical frequency) little can be said about the shape of the total (incident plus reflected) wave spectrum without actually specifying the incident wave field and carrying out the calculation. The object of this section is to demonstrate the drastic changes that result from reflection off a sloping bottom by a typical oceanic internal wave field. The resulting spectral energy density is singular at the critical frequency, a fact that prohibits calculation of the portion of and degree by which the deep-ocean internal wave spectrum is perturbed by bottom reflection.

Since Garrett-Munk (GM) kinematic models of the internal wave spectrum are well established as describing the nearly universal form of internal wave fluctuations in the deep ocean, their most recent version is the obvious choice for a typical incident internal wave field at the ocean bottom. We adopt the point of view that high off the bottom the wave field adjusts itself to the GM-model spectrum which is composed of horizontally isotropic, vertically symmetric fields of upgoing and downgoing waves. The downgoing rays of this spectrum are chosen as the incident field for the bottom-reflection calculation presented here. The upgoing rays are ignored for the moment because they are less likely to be incident with the GM spectrum, since they have already been modified by reflection elsewhere. (They are included in calculations presented in the next section.) An implicit assumption is that the sloping bottom is broad enough to appear long compared to internal wave wavelengths, so that the incident-plus-reflected spectrum is spatially homogeneous. For an isolated topographic feature on the ocean bottom, the actual reflection pattern will be more complicated. We adopt the near-field point of view to avoid dealing with finite topography. The default assumption of a horizontally isotropic incident spectrum is also questionable in cases where currents near the bottom may produce considerable anisotropy in the incident downward field. This effect will also be ignored. In addition, the incident spectrum of downgoing rays cannot be strictly horizontally isotropic at frequencies less than the critical frequency since some ray directions are precluded (by geometry). For this calculation, the portion of the internal wave field at subcritical frequencies not blocked by topography will still be taken as uniformly distributed in azimuth with the same flux per unit horizontal angle as the canonical spectrum over a flat bottom.

The spectrum that will be used here is called GM79, a late model of the original spectrum proposed in the spirit of planned obsolescence in 1972. Its specific form is given by Munk (1981), and is summarized by:

$$E(\sigma, j) = B(\sigma) \cdot H(j) \cdot E \tag{7a}$$

$$B(\sigma) = \frac{2}{\pi} \frac{f}{\sigma} (\sigma^2 - f^2)^{-1/2};$$

$$\int_f^N B(\sigma) d\sigma = 1 - \frac{2}{\pi} \sin^{-1}(f/N) \tag{7b}$$

$$H(j) = (j^2 + j_*^2)^{-1} / \sum_{j=1}^{\infty} (j^2 + j_*^2)^{-1}; \quad \sum_{j=1}^{\infty} H(j) = 1 \tag{7c}$$

where

$$m_j = \frac{j\pi}{b} \left(\frac{N^2 - \sigma^2}{N_0^2 - \sigma^2} \right)^{1/2}$$

is the WKB local vertical wavenumber corresponding to mode j, $j_* = 3$ is a cutoff mode number above which the wavenumber shape is red, $B(\sigma)$ and $H(j)$ are separable frequency and wavenumber shapes and E is a constant prescribing the level of the model spectrum. Through the wave functions, expressions for the energy spectrum (i.e., energy per unit mass per unit frequency bandwidth per unit wavenumber bandwidth) $S_e(\sigma, j)$ can be calculated as

$$S_e(\sigma, j) = b^2 N_0 N E(\sigma, j) \tag{8}$$

where $N_0 = 3$ cph and $b = 1.3$ km are the reference buoyancy frequency and scale height of the stratification, respectively. The total energy integrated over the GM79 spectrum is

$$\frac{\text{total energy}}{\text{mass}} = E b^2 N_0 N [1 - 2\pi^{-1} \sin^{-1}(f/N)]. \tag{9}$$

The specific case to be examined most thoroughly in this paper is reflection from Muir Seamount, a rather steep nearly uniformly sloping ridge some 3 km high, 80 km long and 20 km wide at its base, located at 33°30′N, 62°30′W, northeast of Bermuda. This is one of the cases discussed by Eriksen (1982). Buoyancy frequency N is 0.605 cph roughly halfway up its side. Using this latitude and buoyancy frequency in GM79, total energy per unit mass in internal waves is 5.60×10^{-4} J kg^{-1}. Taking half the waves as downward gives a vertical flux

$$\text{vertical flux} = -\frac{\rho_0}{2} b^2 N_0 N \sum_{j=1}^{\infty} \int_f^N E(\sigma, j) \cdot (\mathbf{c}_g \cdot \mathbf{z}) d\sigma \tag{10}$$

equal to 18.33 mW m^{-2}. Isometric drawings of the incident energy density and downward flux spectra for GM79 at the latitude and stratification for the Muir Seamount region are shown in Fig. 1. The spectra are summed over vertical mode number and integrated in frequency to obtain frequency and wavenumber spectra drawn at low wavenumber and low frequency in the plots, respectively. The spectra

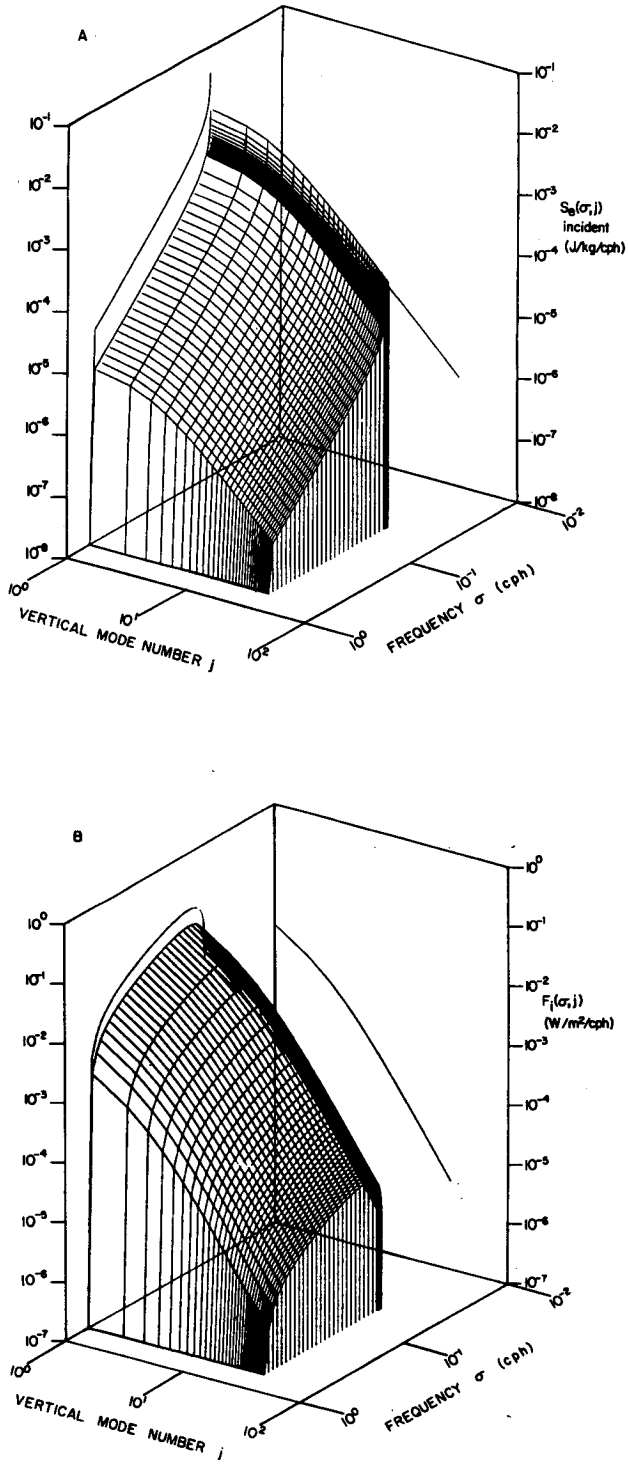

FIG. 1. (a) Energy spectrum $S_e(\sigma, j)$ and (b) flux spectrum $F_i(\sigma, j)$ of downward wave rays incident on a flat bottom ($s = 0$) specified by GM79 with $N = 0.605$ and latitude = 33°30′. Spectra are evaluated on a discrete grid of vertical wavenumbers $j = 1, 32$ and frequencies logarithmically equispaced in two domains above and below $1.1f$, respectively. Unconnected curves drawn in the planes of the ordinate and lowest vertical mode number are frequency spectra; corresponding curves in the opposite plane are wavenumber spectra.

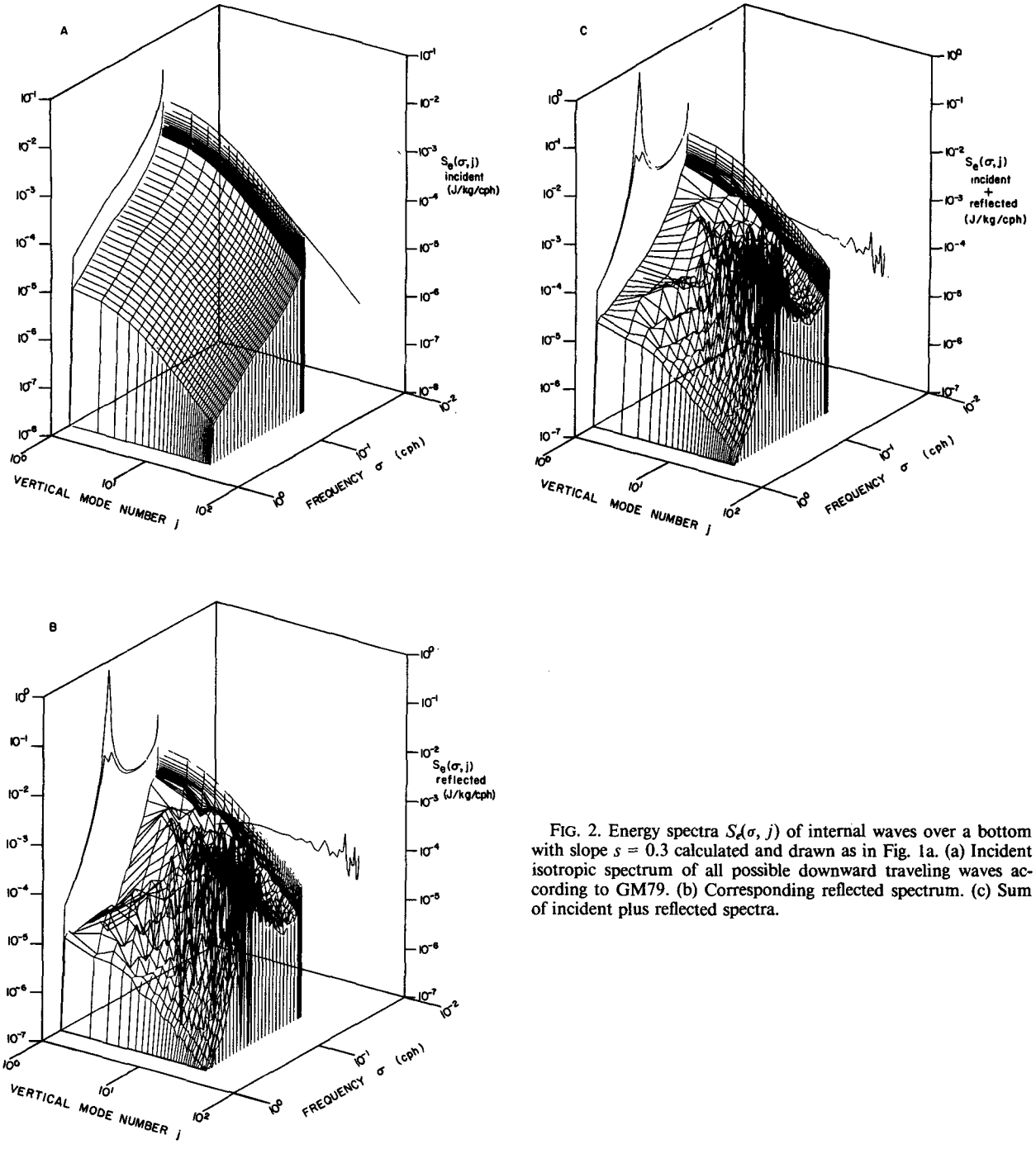

FIG. 2. Energy spectra $S_e(\sigma, j)$ of internal waves over a bottom with slope $s = 0.3$ calculated and drawn as in Fig. 1a. (a) Incident isotropic spectrum of all possible downward traveling waves according to GM79. (b) Corresponding reflected spectrum. (c) Sum of incident plus reflected spectra.

are evaluated for discrete modes $j = 1, 32$ on a frequency grid given by:

$$\sigma_m = \begin{cases} 1.005\sigma_{m-1}, & f \leqslant \sigma_{m-1} < 1.1f \\ 1.10\sigma_{m-1}, & 1.1f \leqslant \sigma_{m-1} < N. \end{cases}$$

These grids were chosen to include more than 95% of the energy in the continuous frequency version of GM79 described above and to extend to moderate vertical mode number without dealing with the details of transition to small scale turbulence (see Munk, 1981; Gargett *et al.*, 1981).

The internal wave spectrum decomposed into incident and reflected parts is shown in Fig. 2 for a bottom slope $s = 0.3$, a typical Muir Seamount value. In these and other calculations presented here, the incident spectrum was spread equally over all azimuths on a 5° grid spacing for numerical integration.

Energy density of reflected waves is summed and represented on the discrete grid of vertical mode numbers according to the computed reflected wavenumber. Reflected wavenumbers corresponding to $j < 1$ are included in the $j = 1$ bin and those corresponding to $j > 32$ are represented in a single high-wavenumber bin not drawn. Two frequency spectra are drawn; the lower one is a sum over $j = 1, 32$ and the higher one includes higher wavenumber reflected components as well. The incident spectrum illustrated in Fig. 2a is the same as in Fig. 1a for supercritical frequencies. The incident spectrum over the slope at subcritical frequencies is lower than that over a flat bottom, more so toward lower frequency, since more and more incident azimuths are blocked by the bottom. The incident spectrum over a slope reaches a value one octave less than the incident spectrum over a flat bottom at $\sigma = f$ (i.e., half the possible azimuths of the GM79 spectrum are blocked when $\sigma = f$).

The reflected spectrum (Fig. 2b) illustrates the loss of low-wavenumber and gain of high-wavenumber energy at nearly all frequencies, but especially near the critical frequency. The reflected wavenumber spectrum is nearly flat in the range $j = 1, 32$ instead of strongly red for $j \gg j_* = 3$. The reflected frequency spectrum is strongly peaked at $\sigma = \sigma_c$ with most of the contribution coming from wavenumbers higher than the $j = 32$ mode. The spectral peak is sharper than a simple pole, that is, it is a nonintegrable singularity. The total spectrum (Fig. 2c, incident plus reflected) looks much like the reflected spectrum, the principal difference being at low mode number. The total spectrum is dominated by the reflected spectrum in a broad frequency band centered on the critical frequency.

The regular sequences of ridges in both Figs. 2b and 2c running diagonally toward higher mode number from $\sigma \approx f$ and $\sigma \approx N$ toward $\sigma = \sigma_c$ are due to enhanced energy in reflected waves caused by incident waves from the gravest and successively higher modes. These ridges are irregular because of the discrete grid of wavenumber bins chosen to draw the calculation. Near $\sigma = \sigma_c$, the reflected spectrum is most irregular. A spectrum continuous in wavenumber would not show these features.

Most of the variance in the spectrum of internal waves over a sloping bottom is contributed by waves at frequencies close to the critical frequency. Since the critical frequency peak is a nonintegrable singularity, it is impossible to estimate the amount of energy involved in the reflection process simply by integrating the spectrum. Another method of making such an estimate is proposed in Section 4.

At both steeper and gentler slopes than used in the example of Fig. 2, the critical frequency is shifted toward one extreme or the other of the internal wave range. The band of frequencies for which the total spectrum is substantially different from that in a flat bottom case is narrower when $\sigma_c \to f$ or $\sigma_c \to N$. A plot of the variation of critical frequency with slope for the pair of parameters f, N appropriate to Muir Seamount is shown in Fig. 3. The critical frequency is asymptotic to either f or N depending on whether $s < f/N$ or $s > 1$, respectively, with a range of nearly linear increase in σ_c with s for $f/N < s < 1$. Slopes as great as unity on the deep ocean floor are rare on the scale of interest, but, for low latitudes, slopes satisfying $s > f/N$ are common. Thus the influence of bottom reflection on internal waves is likely to be most prominent in tropical oceans, but not restricted to them.

4. Flux redistribution implied by observed spectra

In the model discussed in the previous two sections, linear internal wave reflection from a sloping bottom implies gross changes in the energy density of waves. In observations, however, grossly different spectra occur only very close to the ocean bottom and decay roughly exponentially (faster than could be accounted for by geometric spreading of waves from a finite topographic feature). The implication is that the internal wave field redistributes its energy over rather short distances. Some incident internal wave energy is undoubtedly lost to mixing since Richardson numbers are driven down to a limiting value, but the rest presumably is redistributed within the reflected spectrum. Losses to mixing are expected from the fact that shear-variance amplification is proportional to vertical wavenumber amplification to the fourth power.

The linear model discussed so far conserves energy by conserving energy flux normal to a sloping bottom during reflection. Nonlinear processes presumably redistribute reflected wave energy within a few hundred meters of the bottom. Since the observations show that the total internal wave frequency spectrum outside this layer is indistinguishable from the canonical GM model and that reflection imposes wavenum-

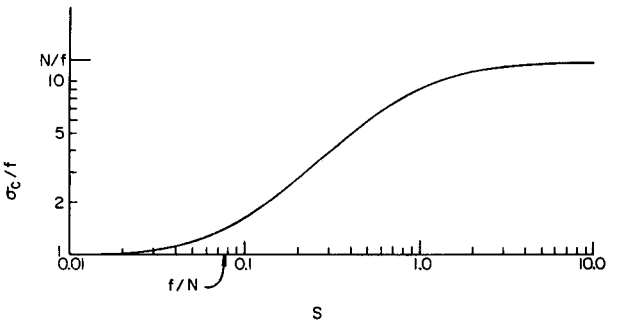

FIG. 3. Critical frequency σ_c vs slope s for N/f corresponding to choices in Figs. 1, 2 and 4. Region of most rapid change in σ_c is $f/N < s < 1$.

ber amplification on components of the wave field, there is an implied energy flux imbalance between the incident and reflected internal wave fields at the top of this layer. A measure of this imbalance is the flux difference between incident wave components whose energy is described by the canonical spectrum and their reflected counterparts (in general, at different wavenumber) which are prescribed to take on amplitudes that are also consistent with the canonical spectrum. The rationale for this calculation is that a reflected component must adjust to the canonical spectral level for its particular wavenumber and frequency in order for the observed total (incident plus reflected) spectrum not to imply a flux imbalance at that particular (reflected) wavenumber and frequency. The difference between incident flux and reflected flux accomplished within a prescribed distance from the bottom is then a measure of the power redistribution per unit volume of the internal wave field.

The calculations that are shown in this section use the incident spectrum $E(\sigma, j)$ developed in the previous section to compute a normal flux into the bottom

$$F_i(\sigma, j, \phi_i) = -\frac{\rho_0}{2} E(\sigma, j)\mathbf{c}_g(\sigma, m_i, \phi_i)\cdot\mathbf{n} \quad (11)$$

where $m_i = j\pi b^{-1}(N^2 - \sigma^2)^{1/2}(N_0^2 - \sigma^2)^{-1/2}$ and ϕ_i are the vertical wavenumber and azimuth of the incident wave as before, and $\mathbf{n} = -\sin\alpha\mathbf{x} + \cos\alpha\mathbf{z}$ is the unit normal into the ocean from the sloping bottom. The reflected normal flux out of the bottom for this component with the prescribed energy density is

$$F_r(\sigma, j', \phi_r) = \frac{\rho_0}{2} E(\sigma, j')\mathbf{c}_g(\sigma, m_r, \phi_r)\cdot\mathbf{n} \quad (12)$$

where j' is the nearest positive integer to $j|m_r/m_i|$ and ϕ_r is the reflected azimuth according to (1) and (2). The spectrum of internal wave flux that is redistributed is the difference magnitude of (11) and (12) integrated over all incident azimuths:

$$F_R(\sigma, j) = \int_0^{2\pi} d\phi_i |F_i(\sigma, j, \phi_i) - F_r(\sigma, j', \phi_r)|. \quad (13)$$

The absolute value is taken because, in general, wavenumber amplification may be greater or less than unity, according to the rules (3). Integrals over azimuth of F_i and F_r give the incident and reflected flux spectrum normal to the boundary. Further integrals over frequency and sums over all j for these quantities and for $F_R(\sigma, j)$ give the total incident, total reflected and total redistributed flux normal to the sloping bottom for the entire wave field.

For the illustrative example of the previous section, these flux spectra are drawn in Fig. 4. The incident spectrum (Fig. 4a) is qualitatively similar to that for a horizontal bottom (Fig. 1b) but there is less roll-off as $\sigma \to f$ since in the sloping bottom case both horizontal and vertical fluxes contribute to the normal flux. The reflected flux spectrum (Fig. 4b) shows a sharp valley centered at $\sigma = \sigma_c$ at all wavenumbers. Obviously, this will be a large source of contribution to the redistributed flux spectrum $F_R(\sigma, j)$. $F_r(\sigma, j')$ also has higher amplitude than $F_i(\sigma, j)$ at low wavenumber and $\sigma > \sigma_c$. This is due to reflection to lower wavenumber. At higher wavenumbers ($j \gtrsim j_*$), the redness of $E(\sigma, j)$ cancels this effect. The redistributed flux spectrum in Fig. 4c indicates the rather broad and powerful implications of reflection on the internal wave field. The $F_R(\sigma, j)$ surface is the same order of magnitude as $F_i(\sigma, j)$. In fact, for this case, the total redistributed flux (34.56 mW m^{-2}) exceeds the total incident flux (30.82 mW m^{-2}) and the total reflected flux (20.39 mW m^{-2}). By this measure, it is clear that virtually all of the internal wave-field flux may be involved in the reflection process and its subsequent redistribution of energy. In contrast to changes in the internal wave spectrum calculated in the previous section, the primary flux imbalances take place at low mode number (nearly all of the flux variance is represented in our grid $j = 1, 32$, even though there are reflected waves at higher wavenumber).

The forms of $F_i(\sigma, j)$, $F_r(\sigma, j)$ and $F_R(\sigma, j)$ change continuously for different slopes s and given f and N while retaining the qualitative features mentioned in describing the particular example presented here. To summarize the variation of total flux integrated over each of these flux spectra, calculations were also made for a variety of slopes $0.01 \leq s \leq 10$ for the same f and N as above for downward, upward and downward/upward ray incidence. The results of these separate calculations are plotted in Fig. 5a–c, respectively. While the total downward incident and reflected fluxes (Fig. 5a) have similar ranges (about 20–50 mW m^{-2}), the total redistributed flux exhibits a broad maximum roughly over the slope range over which σ_c varies nearly linearly (i.e., $f/N \lesssim s \lesssim 1$). Outside this range the redistributed flux varies nearly linearly with s. Inside this range, the total redistributed flux varies between about 20–35 mW m^{-2}. Also shown in Fig. 5a is the difference between total incident and total reflected flux in these calculations. For small slope the reflected flux exceeds the incident flux, because in this limit most of the internal wave range has $\sigma > \sigma_c$ so that reflection to lower wavenumber (greater flux) dominates reflection to higher wavenumber (smaller flux) over most of the range $f < \sigma < N$. For larger slopes, reflection to higher wavenumber dominates (since the incident flux frequency spectrum is red) giving a net flux into the bottom. Upward incident flux F_i (Fig. 5b) increases monotonically with slope since the frequency range for possible upward incidence on the bottom $f < \sigma < \sigma_c$ increases with s as in Fig. 3. The reflected flux F_r for this case exceeds F_i for all s because reflected waves in this

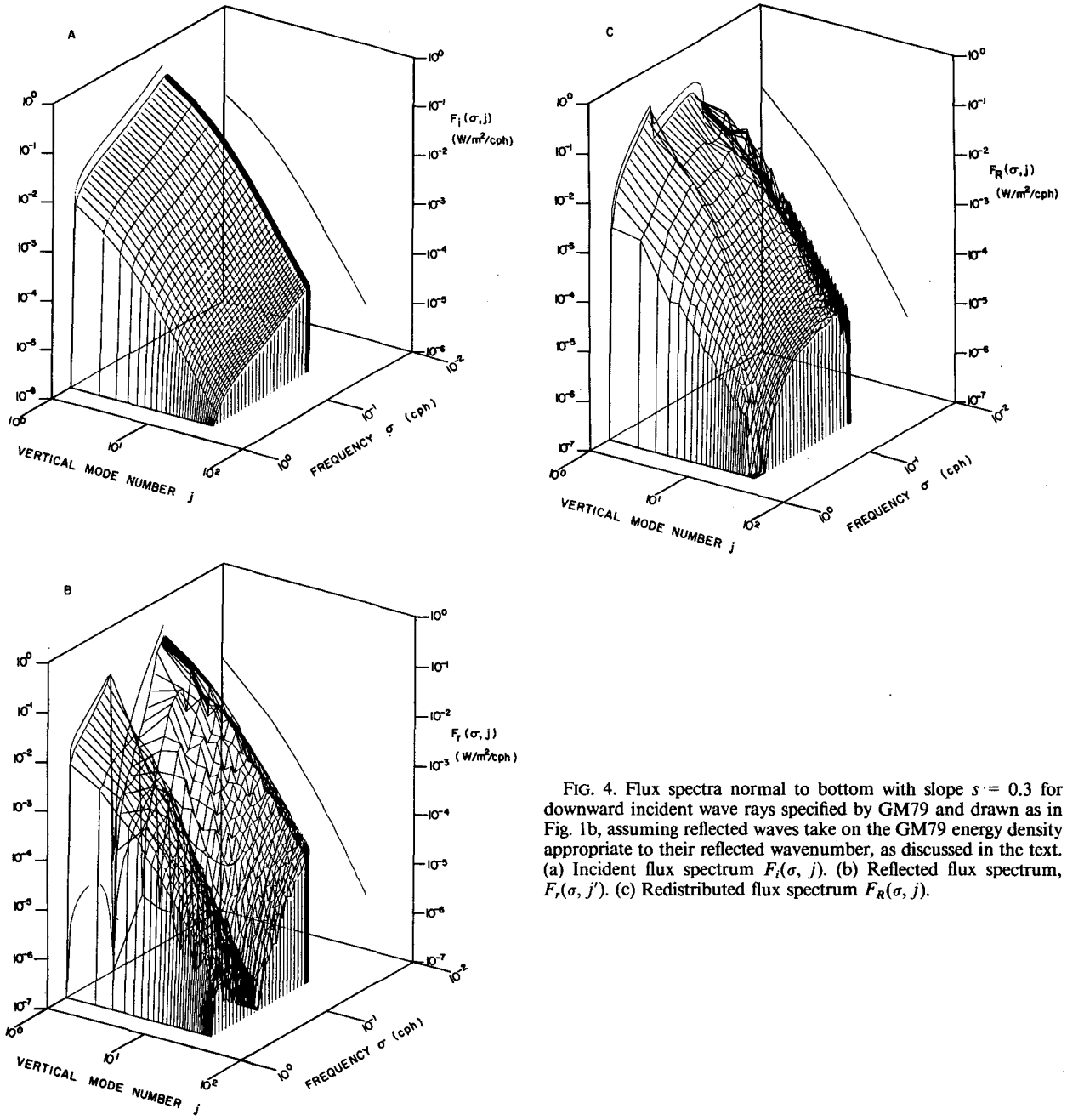

FIG. 4. Flux spectra normal to bottom with slope $s = 0.3$ for downward incident wave rays specified by GM79 and drawn as in Fig. 1b, assuming reflected waves take on the GM79 energy density appropriate to their reflected wavenumber, as discussed in the text. (a) Incident flux spectrum $F_i(\sigma, j)$. (b) Reflected flux spectrum, $F_r(\sigma, j')$. (c) Redistributed flux spectrum $F_R(\sigma, j)$.

case are all longer than their incident counterparts. Redistributed flux for this case is just $F_R = F_r - F_i$ which has a broad maximum of nearly 30 mW m^{-2} centered roughly at $s = 0.5$ (Fig. 5b). When both downward and upward incident fluxes are included together (Fig. 5c), reflected flux exceeds incident flux ($F_r > F_i$) for all s and redistributed flux F_R has a broad maximum near $s = 0.5$ as in the cases of downward or upward incident flux alone; F_R reaches a maximum value of nearly 60 mW m^{-2} which is roughly twice what is contributed by downward or upward incident flux by themselves. The possible significance of $F_r \neq F_i$ is discussed in the next section.

5. Discussion

The relevance of the calculations presented in the previous section to the oceanic internal wave field depends on several assumptions whose validity may be questioned. These range from the appropriateness of linear theory to the choice of parameters that characterize the internal-wave flux spectrum. Com-

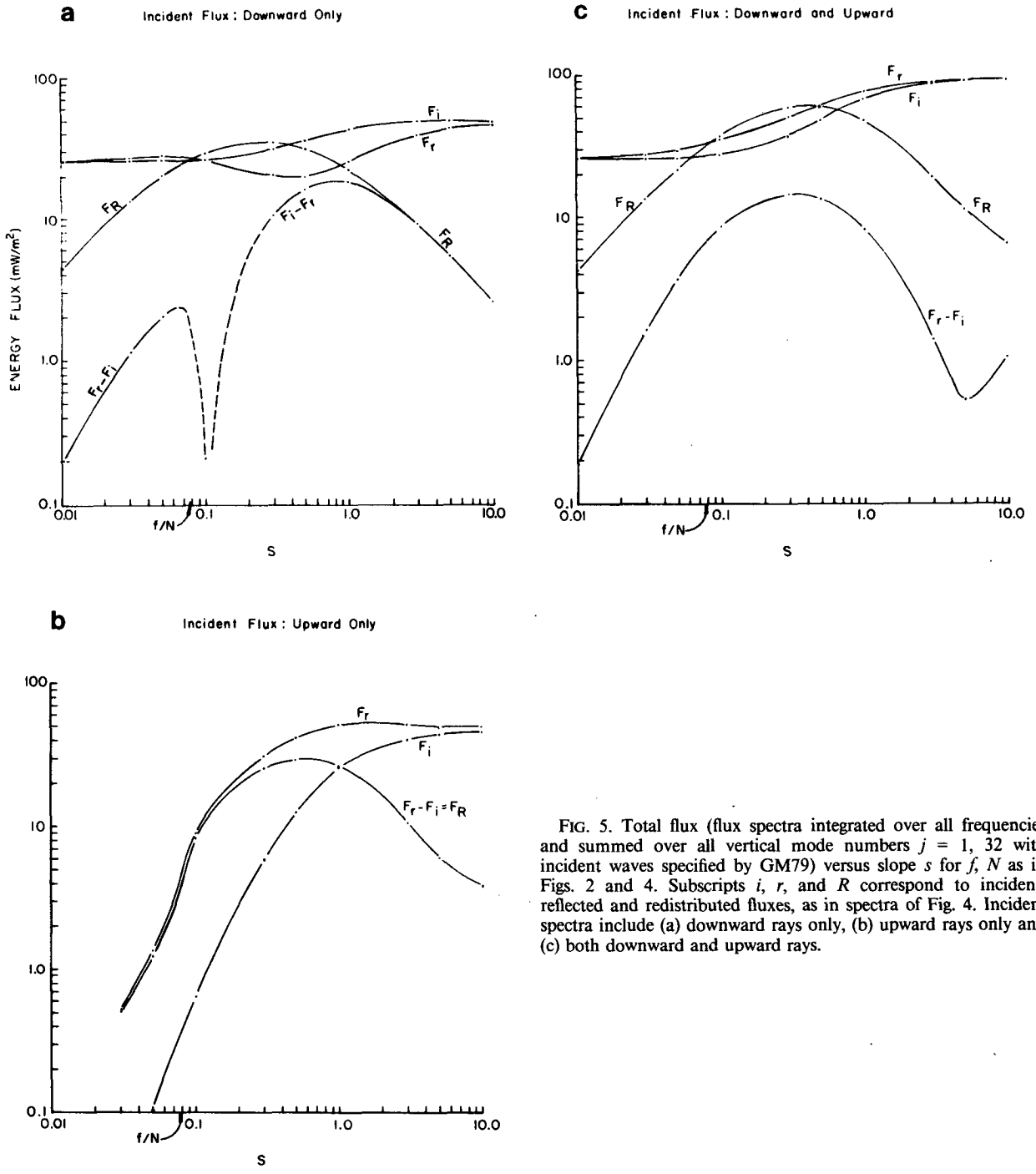

FIG. 5. Total flux (flux spectra integrated over all frequencies and summed over all vertical mode numbers $j = 1, 32$ with incident waves specified by GM79) versus slope s for f, N as in Figs. 2 and 4. Subscripts i, r, and R correspond to incident, reflected and redistributed fluxes, as in spectra of Fig. 4. Incident spectra include (a) downward rays only, (b) upward rays only and (c) both downward and upward rays.

ments on the validity of these assumptions and the implications of the flux-redistribution calculation for internal wave interactions and deep ocean mixing will be presented here.

The relevance of flux estimates calculated assuming linear internal waves is not established observationally, mostly because identification of phase propagation is rather difficult. Several studies of weakly interacting waves have been done for the oceanic internal wave field, but objections to their validity have been raised by Holloway (1980, 1982). Olbers (1983) summarizes these studies. In estimating fluxes associated with various processes, most authors estimate flux by the product of energy density and (linear wave) group velocity, perhaps for want of a better method. In following suit, our flux estimates are at least made in

a manner consistent with others, even if they may not be strictly correct in describing oceanic conditions.

The redistributed flux value attained by integrating the flux spectrum depends on various parameterizations of the wave field. In particular, it depends on latitude in two ways. As mentioned, the redistributed flux varies relatively weakly with slope s for given f and N. Since observations suggest that the level of the oceanic internal wave spectrum is relatively independent of latitude and buoyancy frequency (rather than being proportional to f, as in GM79; see footnote 14 of Munk, 1981), the total flux of the wave field varies roughly inversely as f. In addition, the closer s falls to the range $f/N < s < 1$, the larger the flux redistribution will be for given f and N. Thus latitudes $\theta \leqslant \sin^{-1}(sN/2\Omega)$, where Ω is the earth's rotation rate, are likely to be the sites of greatest flux redistribution. For typical values ($s \sim 0.07$, benthic $N(z) \sim 0.5$ cph), this leads to $\theta \leqslant 25°$, which corresponds to roughly half of the world ocean. The other important parameterization of the wave field is energy content at the gravest vertical scales. Since we use vertical wavenumbers specified by $m = j\pi b^{-1}(N^2 - \sigma^2)^{1/2}(N_0^2 - \sigma^2)^{-1/2}$, $j = 1, 32$, the form of $H(j)$ coupled with $c_g \alpha j^{-1}$ causes most flux to be contributed by only the lowest few modes ($j \leqslant j_*$) of the spectrum. If, for some reason, these long wavelengths are not part of the incident spectrum, the incident (thus redistributed) flux will be accordingly smaller. The low-wavenumber form of GM79 has not been verified observationally, so the incident flux employed in the reflection calculations is uncertain. However, since theoretical calculations by others also assume GM79 as a canonical spectrum, the results from this study are on an equal basis. That is, although the flux redistributions calculated here may be different from those in the actual ocean, their relative value compared to other theoretically postulated fluxes is consistent.

Flux calculations that involve reflection to smaller wavenumber are subject to dispute because reflected flux has been estimated by assuming reflected waves have vertical scales that are very long ($m_r/m_i \to 0$). Since flux varies as m^{-1}, the longest reflected waves dominate reflected flux. These waves may be much longer than those of the gravest mode ($j = 1$) of the incident wave field; thus the ocean surface is really in the near-field for the reflection process and simple linear ray theory is inappropriate. As (3) states, all upward incident flux ($m_i < 0$, $\sigma < \sigma_c$) and azimuths $|\phi_i| \geqslant \cos^{-1}(-s \tan\theta_i)$ have $|m_r/m_i| \leqslant 1$.

Redistributed flux F_R is a better measure of how much wave flux must be converted from one wavenumber to another as a result of reflection than the net difference $F_i - F_r$. To illustrate this, consider a special case of two incident waves of the same vertical wavenumber and frequency, but different azimuth such that the excess of incident over reflected flux for the wave that reflects to higher wavenumber is equal to the excess of reflected over incident flux for the wave that reflects to lower wavenumber. The net flux is zero in this case, but flux redistribution clearly takes place within the spectrum and has a value twice that due to either wave alone.

These calculations ignore any dynamical effect of a mixed layer at the ocean bottom on internal wave reflection. This is a reasonable assumption since incident wave scales are long compared to typical benthic boundary layer thicknesses. D'Asaro (1982) and Fu (1981) both show that such a layer over a flat bottom is highly reflecting to near-inertial waves of realistic vertical scale. The experimental study of Cacchione and Wunsch (1974) indicates that internal wave reflection occurs despite the presence of a mixed layer at the sloping boundary. Energy flux changes due to reflection may provide a source for mixing the ocean near a sloping boundary. This possibility is considered below.

The partition between energy lost from the internal wave field to mixing and energy simply redistributed within the spectrum requires an extension to the reflection model. No such extension will be offered here, only a reminder that shears become sufficiently high in reflection to drive Richardson numbers to very low values. Following Munk (1981) we define an inverse Richardson function

$$\mathrm{Ri}^{-1}(j_u) = \sum_{j=1}^{j_u} \int_f^N (S_{u_z}(\sigma, j)/N^2) d\sigma \qquad (14)$$

which is the inverse Ri resulting from a shear spectrum S_{u_z} summed to upper mode number j_u. Since $S_{u_z} = m^2(\sigma^2 + f^2)\sigma^{-2} S_\epsilon(\sigma, j)$, it is clear that $\mathrm{Ri}^{-1}(j_u)$ will reach a fixed value (say, unity) for a lower j_u for waves reflecting off a sloping bottom than off a flat one. Just as with the energy spectrum, though, $\mathrm{Ri}^{-1}(j_u) \to \infty$ as $\sigma \to \sigma_c$ *independent* of j_u because of the (nonintegrable) singularity in $S_\epsilon(\sigma, j)$. Whereas in the flat bottom case most shear variance is contributed by near-inertial frequencies, over a sloping bottom most of the shear is near the critical frequency σ_c. Thus most mixing events should take place at a preferred frequency $\sigma \approx \sigma_c$ and near the bottom. Unlike the interior case, breaking due to bottom reflection can be expected locally in depth (near the bottom) but not in time. Rather, it should be local in frequency, instead. Such periodic near-bottom mixing does occur in laboratory experiments of critical frequency reflection (Cacchione and Wunsch, 1974).

A reviewer has suggested an alternate model for computing the amount of energy flux involved in the reflection process. In this model, an incident energy density spectrum has upper wavenumber cutoff j_u specified by the condition $\mathrm{Ri}^{-1}(j_u) = 1$. The reflected spectrum is partitioned in wavenumber into a part for which $\mathrm{Ri}^{-1}(j_p) = 1$ and one for which

$$\int_f^N \sum_{j=j_p}^{j'_u(\sigma)} (S_{u_z}(\sigma, j)/N^2) d\sigma \to \infty$$

where $j'_u(\sigma)$ is the upper wavenumber limit that is determined by j_u of the incident spectrum and its amplification by reflection. The part of the reflected spectrum with $j < j_p$ must tend to zero as $\sigma \to \sigma_c$ since all incident wavenumbers $j = 1, j_u$ tend to infinity in this limit. The difference between incident normal flux and low-wavenumber ($1 \leq j \leq j_p$) reflected flux then gives a measure of how much energy flux occurs at high wavenumbers $j > j_p$ in the reflected field. This is so because flux normal to the sloping bottom is conserved in this model, as in the discussion in Section 3. Unfortunately, the partition at $j = j_p$ does not necessarily divide the reflected spectrum into a part that accounts exclusively for loss of wave energy to mixing (say $j < j_p$) and one that does not, independent of the definition $\mathrm{Ri}^{-1}(j_p)$ = constant. Mixing events are typically local in depth rather than in vertical wavenumber. Waves of different, even disparate, wavenumber superpose randomly to create overturning so that the whole of the wave spectrum (incident plus reflected) potentially contributes to mixing. Once the total spectrum must be considered, the problem of the singularity in S_e impedes estimation of energy flux involved in mixing (or any other spatially local process) due to reflection.

The range of redistributed flux in the examples we have used is about 3–60 mW m^{-2} for $0.01 < s < 10$, but also at least 20 mW m^{-2} for $f/N < s < 1$. This is very large compared to estimates for generation, spectral transfer, or dissipation mechanisms for internal waves. It exceeds the estimates for individual mechanisms of these three processes by an order of magnitude according to Olbers (1983). Observations suggest that this flux redistribution must take place over O(100 m) vertically, as was mentioned above.

Internal waves have long been examined as an agent of mixing the deep ocean to produce the basin-wide vertical diffusivities needed to maintain the thermocline in balance with mean vertical advection. Garrett (1979a) reviewed the mechanisms proposed to produce the desired "classical" value of 10^{-4} m^2 s^{-1}, finding "no clear answers yet to the problems of understanding and parameterizing vertical mixing in the ocean." Internal waves in the deep ocean interior do not appear to provide enough mixing to account for the desired diffusivity. Both Garrett (1979a) and Armi (1978), like Munk (1966), suggested that boundary mixing across isopycnals coupled with horizontal mixing by mesoscale eddies provides the needed effective mixing. Armi (1978) proposed turbulent bottom drag as a mechanism for boundary mixing, but Garrett (1979b) objected that his formula could correspond to more than 100% efficiency of conversion of kinetic to potential energy. In reply, Armi (1979) suggested roll waves or obstacle wakes as other mechanisms, but without a model for their mixing efficacy. His observations of deep mixed layers detached from the bottom and chemical tracer distributions in them strongly suggest that robust mixing at topographic features is, in fact, taking place.

Internal wave reflection off a sloping bottom may well provide the desired mixing mechanism. If a fraction ϵ of the total redistributed flux F goes in to potential energy change, the average rate of potential energy creation is $\epsilon FA/V$ where A is the area over which the flux is applied to the volume V. This can be regarded as a topography-weighted rate of potential energy creation. It is equal to the effective vertical diffusivity K times $\rho_0 N^2$, where turbulent buoyancy flux has been parameterized by turbulent diffusion. Thus

$$K = \epsilon FA/\rho_0 V N^2. \tag{15}$$

Notice that flux F is proportional to $S_e(N^2 - f^2)/m$ [see (6)]. For $f \ll N$, $F \propto N^2(z)$ so that K is independent of N. If A is the ocean-basin bottom area and V is its total volume, the ocean-averaged effective vertical diffusivity can be calculated for this mechanism just as in the calculations of Armi and Garrett. For typical basin-averaged values, $A/V \sim (\text{depth})^{-1}$ and $N \sim 1$ cph, giving

$$K \sim \epsilon \cdot 1.3 \times 10^{-3} \text{ m}^2 \text{ s}^{-1}$$

for $F = 20$ mW m^{-2} and depth = 5 km. This implies that only an efficiency of 8% is needed to provide the desired basin-averaged vertical diffusivity of 10^{-4} m^2 s^{-1}. Estimates for production of potential energy from shear instability are 20% or less (Thorpe, 1973)—although viscous effects in the laboratory experiments used to make this estimate cast it in some doubt (Thorpe, personal communication, 1984). Thus only about 40% of the total redistributed flux F need undergo shear instability in order to produce enough mixing. (The remaining flux presumably rejoins the internal wave spectrum.) As mentioned before, the absolute magnitude of flux is not well known. Therefore, this is really an order of magnitude calculation. The details of the distribution of bottom slopes in the ocean suggest that mixing by this mechanism is likely to be geographically dependent. Nevertheless, the calculation is in the fortunate position of needing a rationale to reduce ϵ, rather than increase F, to get the desired result.

By these calculations it appears that internal wave reflection off rough topography of the world's ocean basins is a likely mechanism for boundary mixing, and is, as such, the likely link in effecting basin-scale vertical diffusivity via the boundaries.

Acknowledgments. Christopher Garrett, as well as the prospect of spending a few January days in Hawaii, renewed my curiosity in internal wave reflection off sloping bottoms. I thank Chris and my other

colleagues at the 'Aha Huliko'a Hawaiian Winter Workshop on internal gravity waves and small-scale turbulence for their helpful comments on this work. I am grateful to the U.S. Office of Naval Research for support for this work under Contract N00014-809-C-0273.

REFERENCES

Armi, L., 1978: Some evidence for boundary mixing in the deep ocean. *J. Geophys. Res.*, **83,** 1971–1979.

——, 1979: Reply to comments by C. Garrett. *J. Geophys. Res.*, **84,** 5097–5098.

Bell, T. H., Jr., 1975a: Topographically generated internal waves in the deep ocean. *J. Geophys. Res.*, **80,** 320–327.

——, 1975b: Statistical features of sea-floor topography. *Deep-Sea Res.*, **22,** 883–892.

Cacchione, D., and C. Wunsch, 1974: Experimental study of internal waves over a slope. *J. Fluid Mech.*, **66,** 223–239.

D'Asaro, E., 1982: Absorption of internal waves by the benthic boundary layer. *J. Phys. Oceanogr.*, **12,** 323–336.

Eriksen, C. C., 1982: Observations of internal wave reflection off sloping bottoms. *J. Geophys. Res.*, **87,** 525–538.

Fu, L.-L., 1981: Observations and models of inertial waves in the deep ocean. *Rev. Geophys. Space Phys.*, **19,** 141–170.

Gargett, A. E., P. J. Hendricks, T. B. Sanford, T. R. Osborne and A. J. Williams, III, 1981: A composite spectrum of vertical shear in the upper ocean. *J. Phys. Oceanogr.*, **11,** 1258–1271.

Garrett, C., 1979a: Mixing in the ocean interior. *Dyn. Atmos. Oceans,* **3,** 239–265.

——, 1979b: Comment on "Some evidence for boundary mixing in the deep ocean" by Laurence Armi. *J. Geophys. Res.*, **84,** p. 5095.

Hogg, N. G., E. J. Katz and T. B. Sanford, 1978: Eddies, islands, and mixing. *J. Geophys. Res.*, **83,** 2921–2938.

Holloway, G., 1980: Oceanic internal waves are not weak waves. *J. Phys. Oceanogr.*, **10,** 906–914.

——, 1982: On interaction time scales of oceanic internal waves. *J. Phys. Oceanogr.*, **12,** 293–296.

Johnson, C. L., and T. B. Sanford, 1980: Anomalous behavior of internal gravity waves near Bermuda. *J. Phys. Oceanogr.*, **10,** 2021–2034.

Munk, W. H., 1966: Abyssal recipes. *Deep-Sea Res.*, **13,** 207–230.

——, 1981: Internal waves and small scale processes. *Evolution of Physical Oceanography Scientific Surveys in Honor of Henry Stommel.* B. A. Warren and C. Wunsch, Eds., MIT Press, 264–291.

Olbers, D. J., 1983: Models of the oceanic internal wave field. *Rev. Geophys. Space Phys.*, **21,** 1567–1606.

Thorpe, S. A., 1973: Turbulence in stably stratified fluids: A review of laboratory experiments. *Bound. Layer Meteor.*, **5,** 95–119.